WATER RESOURCES RESEARCH, VOL. 49, 2437–2445, doi:10.1002/wrcr.20212, 2013

Mapping large-scale river flow hydraulics in the Amazon Basin

Augusto C. V. Getirana[1] and Rodrigo C. D. Paiva[2,3]

Received 26 June 2012; revised 21 March 2013; accepted 24 March 2013; published 17 May 2013.

[1] Research on actual requirements for a numerically consistent representation of flow dynamics in large-scale river-flood models are needed to improve both modeling performance and computational efficiency. Still, regional- and global-scale characterizations of river hydrodynamics are absent. A first attempt to map river hydrodynamics in the Amazon Basin is presented. Flood wave type maps at 0.25° spatial resolution are derived from a classification method based on the analysis of *Saint-Venant* equation terms. Global river geometry data sets derived from both digital elevation models and empirical equations supported by stream gauge observations are used as input variables. Errors of input variables are estimated, and a sensitivity analysis is performed. Results show that 64.5% of rivers (headwaters and high-slope rivers) can be represented by the kinematic wave (KI), 34.5% (main Amazon tributaries, low slope, and wetland regions) by the diffusive wave (DF), and 1% (lower Amazon) by the full Saint-Venant equations (SV). In a rigorous scenario, i.e., a case where the most restricted classification of each grid cell is considered, ∼33% is classified as KI, ∼62% as DF, and ∼5% as SV. Most of the basin presents subcritical flow with very low Froude number (*Fr*), while the Andean region is dominated by larger *Fr* values and supercritical flow can be found. According to our evaluation mostly based on in situ data, the map has a percentage of detection of 83.4%.

Citation: Getirana, A. C. V., and R. C. D. Paiva (2013), Mapping large-scale river flow hydraulics in the Amazon Basin, *Water Resour. Res.*, *49*, 2437–2445, doi:10.1002/wrcr.20212.

1. Introduction

[2] River flow dynamics plays an important role in terrestrial water cycle and global earth system. It regulates freshwater discharge from land into oceans [*Oki and Kanae*, 2006], extent of flooded areas [*Papa et al*., 2010], and consequently, land-atmosphere exchanges of water, energy [*Krinner*, 2003; *Decharme et al*., 2011], and gases such as methane [*Gedney et al*., 2004]. Moreover, it directly affects human beings due to their vulnerability to floods and droughts.

[3] Large-scale river-flood models are one of the main predictive tools of river flow dynamics. Although the *Saint-Venant* equations [*Cunge et al*., 1980] presumably provide the most complete 1-D description of river hydrodynamics, most of the recent modeling developments use simplified forms of these equations, with some exceptions [e.g., *Paiva et al*., 2013a, 2013b]. Since the use of full Saint-Venant equations results in additional computational costs and input data constrains, the momentum conservation law is usually replaced, sorted by increasing model complexity, by simplistic relations between water volume storage within a river reach and its outflow [*Vorosmarty et al*., 1989; *Liston et al*., 1994; *Arora et al*., 1999; *Coe et al*., 2008], kinematic wave or Muskingum-Cunge type methods [*Collischonn et al*., 2007; *Decharme et al*., 2011; *Getirana et al*., 2012], or diffusive wave models [*Yamazaki et al*., 2011]. As a consequence, important hydrologic processes may be neglected depending on how simplified these equations are. Delayed flood peaks and slower increases in water levels are some implications on the physical processes. Longer simulation times are other disadvantages when inappropriate equations are used [*Neal et al*., 2012]. In the Amazon River Basin, for example, backwater effects regulate the flow dynamics in the downstream reaches of main rivers. As examples of these effects in the basin, we can cite (1) the physical influence of sea tides identified at more than 1000 km upstream the river mouth [*Kosuth et al*., 2009], (2) the influence of the main Amazon River on its tributaries' water levels [*Meade et al*., 1991], and (3) the impact of different water slope conditions on flow recession, affecting droughts in the main stream [*Tomasella et al*., 2010]. Even so, this hydraulic characteristic is not represented in the majority of models applied in this basin.

[4] The research for a better understanding of flow dynamics in large rivers has motivated the development and application of complex hydrologic and hydrodynamic models. For example, a previous study on the Amazon River's hydraulic behavior [*Meade*, 1991] inspired several other ones [e.g., *Trigg et al*., 2009; *Yamazaki et al*., 2011; *Paiva et al*., 2013a, 2013b] to use more complete formulations of the Saint-Venant equations in order to better represent

[1]Hydrological Sciences Lab, NASA Goddard Space Flight Center, Greenbelt, Maryland, USA.
[2]Instituto de Pesquisas Hidráulicas, Universidade Federal do Rio Grande do Sul, Porto Alegre, Brazil.
[3]Geosciences Environnement Toulouse, UMR 5563, Université Toulouse III Paul Sabatier, Toulouse, France.

Corresponding author: A. C. V. Getirana, Hydrological Sciences Lab, NASA Goddard Space Flight Center, Greenbelt, MD 20771, USA. (augusto.getirana@nasa.gov)

0043-1397/13/10.1002/wrcr.20212

complex physical processes such as backwater effects, not included in previous river flow simulations in the basin. Sometimes, however, such complex formulations may not be needed in certain regions, and simplifications can be applied for modeling efficiency. In this sense, the a priori knowledge of the most important river hydrodynamic characteristics can be an important factor to guide the improvement of large-scale river-flood models. The present paper addresses this issue by describing and evaluating a robust approach that allows one to classify flow dynamics at the large scale.

[5] Previous studies have suggested different methods to classify river hydrodynamic characteristics and providing information of which simplified form of Saint-Venant can be properly employed for a given river reach [e.g., *Vieira*, 1983; *Moussa and Bocquillon*, 1996]. Other experiences have applied these methods to single river reaches in the Amazon River [*Trigg et al*., 2009]. But a full characterization of river flow dynamics at a regional or global scale is absent. In this paper, we present a spatially distributed (0.25° × 0.25°) flow dynamics' characterization of Amazonian rivers in terms of flood wave type based on the *Moussa and Bocquillon* [1996] method, global data sets, and in situ observations. We also present a Froude number map where the presence of subcritical or supercritical flows can be identified. Results are evaluated based on both the probability of flood wave types to occur in each grid cell and the comparison against results obtained using in situ observations.

2. River Flow Dynamics

[6] Saint-Venant equations, which represent the 1-D gradually varied unsteady flow in open channels through simplifications applied to the *Navier-Stokes* equations, provide the most complete 1-D description of river hydrodynamics. They are composed by the mass and the momentum conservation laws [*Cunge et al*., 1980]:

$$\frac{\partial Q}{\partial x} + \frac{\partial A}{\partial t} = 0 \tag{1}$$

$$\underset{\text{(i)}}{\frac{\partial Q}{\partial t}} + \underset{\text{(ii)}}{\frac{\partial}{\partial x}\left[\frac{Q^2}{A}\right]} + \underset{\text{(iii)}}{gA\frac{\partial y}{\partial x}} = \underset{\text{(iv)}}{gAS_0} - \underset{\text{(v)}}{gAS_f}, \tag{2}$$

where Q ($m^3\ s^{-1}$) is the river discharge, t (s) is time, x (m) is the river longitudinal space coordinate, y (m) is the water depth, g ($m\ s^{-2}$) is the acceleration due to gravity, A (m^2) is the cross-sectional flow area perpendicular to the flow direction, and S_0 ($m\ m^{-1}$) and S_f ($m\ m^{-1}$) are the bed slope and friction slope in the x direction, respectively.

[7] The momentum conservation law (equation (2)) is basically the balance of (i) local and (ii) convective inertia with (iii) pressure, (iv) gravity, and (v) friction forces. The full Saint-Venant system can be simplified, giving rise to different wave models, depending on which terms of equation (2) can be assumed negligible if compared to the others [*Moussa and Bocquillon*, 1996]:

[8] (1) kinematic wave (KI): terms (iv) and (v)

[9] (2) diffusive wave (DF): terms (iii)–(v)

[10] (3) steady dynamic wave (SD): terms (ii)–(v)

[11] (4) gravity wave (GV): terms (i)–(iii).

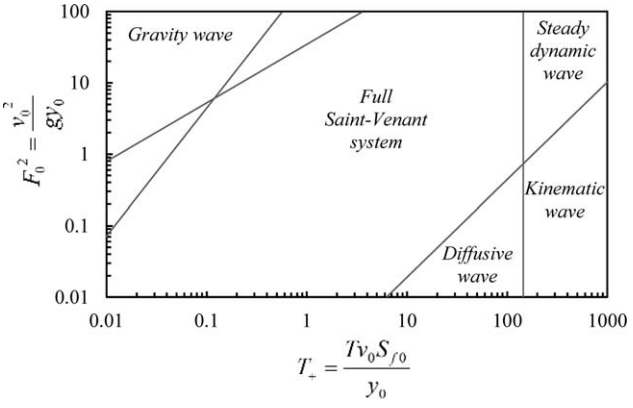

Figure 1. Criteria for flood wave type classification from *Moussa and Bocquillon* [1996].

[12] Aiming to classify river flow according to the flood wave type, we used an approach developed by *Moussa and Bocquillon* [1996] (Figure 1). The approach analyzes the flow using Saint-Venant equations as the superposition of two regimes: a permanent regime and a perturbation of the steady uniform flow. Any term of the momentum equation corresponding to less than 1% of the sum of all terms is neglected, resulting in one of the four simplified flood wave types described earlier. The criterion is applied using two descriptive parameters, the Froude number (F_0) of the unperturbed flow and the dimensionless period (T_+) of the steady-flow perturbation:

$$F_0{}^2 = \frac{v_0{}^2}{g y_0} \tag{3}$$

$$T_+ = \frac{T_0 v_0 S_{f0}}{y_0}, \tag{4}$$

where v_0, y_0, and S_{f0} are the flow velocity ($m\ s^{-1}$), water depth (m), and friction slope ($m\ m^{-1}$) of the unperturbed flow, respectively, and T_0 is the period of perturbation (s). The Froude number is usually defined as the ratio between inertia and gravitational forces, and the flow is defined as subcritical when $Fr < 1$ or supercritical, otherwise. The input parameters for F_0 and T_+ (v_0, y_0, S_{f0}, and T_0) were estimated based on global data sets and in situ observations, as described in the next section.

3. Global- and Large-Scale Data Sets

[13] The spatial resolution of the data set used in this study was chosen in order to understand flood wave regimes in large rivers (in the order of 10^4 km^2 or more) with potential global applications and to support further developments of large- and global-scale models. Based on these objectives, we developed our analyses at the 0.25° spatial resolution, which is also in accordance with currently available regional and global data sets.

[14] The following global parameters were used: the upstream drainage area (km^2), the length of main river L (km), the valley slope of the entire catchment Slp ($m\ m^{-1}$), the river width W (m), the mean annual discharge Q_{mean} ($m^3\ s^{-1}$), the mean upstream flooded area A_{fld} (%), and the

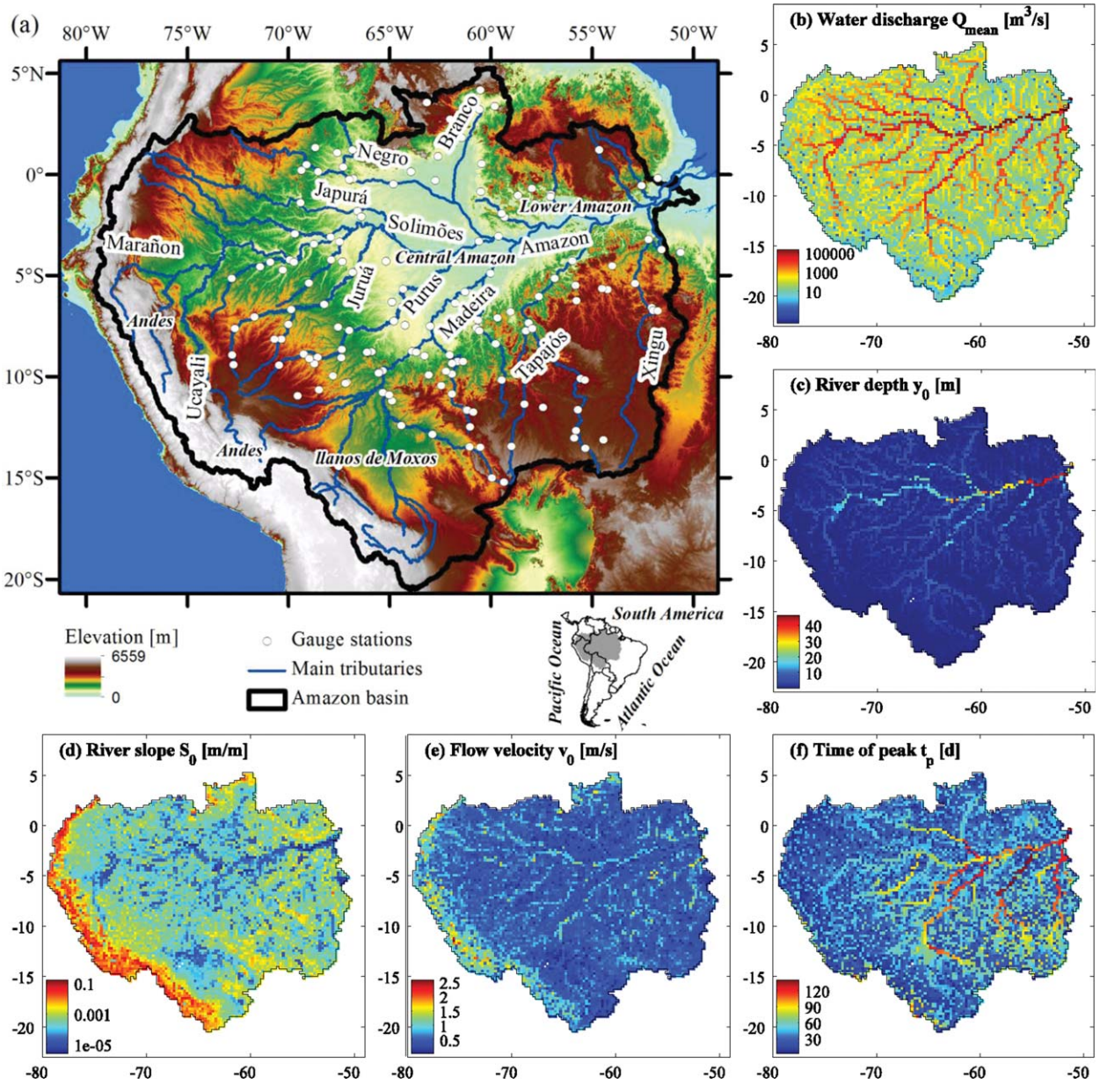

Figure 2. The Amazon Basin: (a) main tributaries and stream gauges (white dots), (b) mean discharge (Q_{med}), (c) river depth (y_0), (d) local surface water slope (S), (e) mean flow velocity (v_0), and (f) time to peak (t_p).

number of months where 90% of annual precipitation occurs P_{90} (months). The Flexible Location of Waterways (FLOW) method [*Yamazaki et al*., 2009] was used to upscale the upstream drainage area (A), river length (L), and water slope (S) at the study resolution (see Figure 2d). The high-resolution flow direction map used by FLOW is given by the 1 km resolution Global Drainage Basin Database [*Masutomi et al*., 2009], which is based on the Shuttle Radar Topography Mission (SRTM) digital elevation model (DEM). SRTM DEM error removal was performed as much as possible before the application of the FLOW algorithm, as described in *Yamazaki et al*. [2012]. The parameter W was estimated using the empirical relationship at the global scale: $W = \max(10, \beta Q_{mean}^{0.5})$ suggested by *Getirana et al*. [2012]. The parameter β is a dimensionless coefficient defined for five different hydrologic regions of the world and is equal to 18 in equatorial or subtropical basins, including the Amazon. The parameter Q_{mean} was estimated for each 0.25° grid cell using the global runoff database from *Cogley* [2003] (see Figure 2b). A_{fld} was derived from the Global Lakes and Wetland Database product [*Lehner and Döll*, 2004] at 30-arcsec resolution (~1 km at the equator). The parameter P_{90} was obtained from the Climatic Research Unit CL 2.0 data set [*New et al*., 2002], which provides 10 min spatial resolution grids of the monthly climatology based on interpolated data from ground stations for the 1960–1990 period. The parameter P_{90} is computed for each grid cell based on the mean rainy season of its own drainage area.

[15] Daily observations of water discharge for the 36 year period (1970–2005) at 156 gauging stations within the

Amazon Basin and about 25,000 instantaneous observations of flow velocities v_0 (m s^{-1}) and river depths y_0 (m) at 255 stations were considered in this study. The data were provided by the Brazilian Water Agency (*Agência Nacional de Águas*, ANA), and the spatial distribution of the stations is given in Figure 2a.

4. Practical Implementation

4.1. Time-to-Peak Calculation

[16] The period of perturbation T_0 was considered as the time to peak (t_p), defined here as the time needed for the river to switch from a low water condition to the flow peak during a flood event. *Moussa and Bocquillon* [1996] estimated T_0 from input hydrographs from single flood events in a single river reach by fitting a sinusoidal function. The identification of single flood events from multiyear large-scale data sets can be a difficult task. In this sense, an automated method was developed to derive t_p from hydrographs. The method considers that both t_p and T_0 values have the same order of magnitude at the log scale, as required in the flood wave classification method, and related limitations are addressed in the sensitivity analysis as described in section 4.3. The procedure to estimate t_p values distributed along the Amazon River Basin was divided into three steps: (1) estimation of the t_p values in stream gauging stations from daily discharge observations, as described in the previous section, (2) development of a statistical model for t_p using multiple explaining parameters, and (3) application of the equation for the whole Amazon Basin. The algorithm used to estimate t_p follows the subsequent steps, as illustrated in Figure 3a: (i) definition of discharge thresholds for low (Q_{min}) and high (Q_{max}) water conditions (after performing a sensitivity analysis, we opted for using 30% and 70% percentiles of daily discharge, respectively); (ii) selection of points in the hydrograph of minimum discharge: $Q(t) < Q_{min}$, $Q(t) < Q(t+1)$ and $Q(t) < Q(t-1)$; (iii) selection of points of maximum discharge: $Q(t) > Q_{max}$, $Q(t) > Q(t+1)$ and $Q(t) > Q(t-1)$; (iv) selection of pairs of subsequent minimum and maximum discharge points from (ii) and (iii) steps; (v) computation of t_p for each pair from (iv) as the distance from points in time; and (vi) finally, t_p equals the mean of the values obtained in (v). Multiple regression analyses were performed to develop a statistical model for t_p using six explaining parameters: A, L, Slp, Q_{mean}, P_{90}, and A_{fld}. The parameters were extracted for each gauging station, and to avoid unnecessary or cross correlated explaining variables, we used the stepwise regression method [*Draper and Smith*, 1998] to derive the best statistical model for the data:

$$t_p = 7.3618 \cdot A^{0.2560} \cdot \mathrm{Slp}^{-0.3036} \cdot P_{90}{}^{-1.4662} \quad (\mathrm{MAE} = 44\%), \quad (5)$$

where MAE is the mean absolute error between observed and regression t_p values. According to equation (5), only A, Slp, and P_{90} showed significant correlation to explain t_p at selected gauging stations, and the other parameters (L, Q_{mean}, and A_{fld}) were rejected by the regression method. The t_p estimates for the Amazon Basin are shown in Figure 2f. As one can see in Figure 3b, the resulting formula is better adapted to large basins than previous ones [*Kiprich*, 1940;

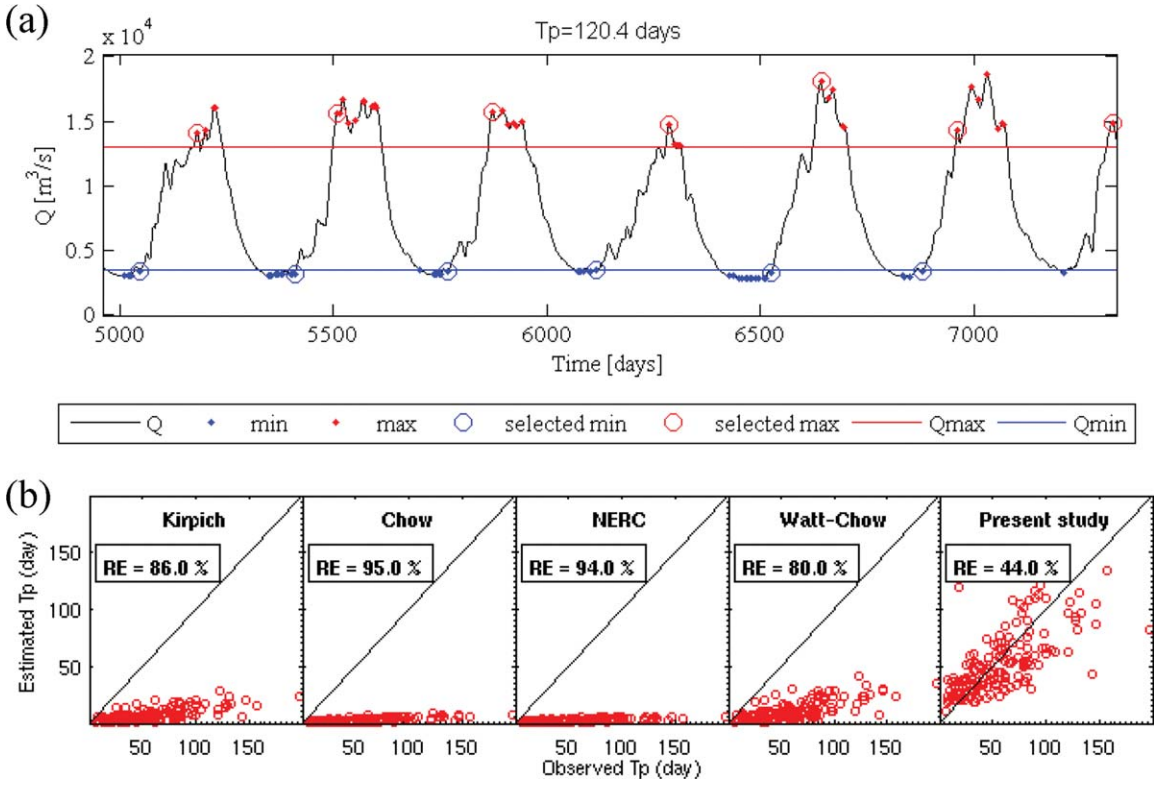

Figure 3. Time-to-peak (t_p) calculation: (a) example of the automated method to define observed t_p from hydrographs and (b) comparison of estimated and observed time-to-peak values derived from different equations.

Chow, 1962; *Natural Environment Research Council*, 1975; *Watt and Chow*, 1985] when t_p estimates are compared against observations at gauging stations located within the Amazon Basin. This is explained by the fact that previous equations were derived for small catchments. More or less complex equations can be found in the literature. Some of them use soil characteristics such as soil conductivity [*Loukas and Quick*, 1996] or other information rarely obtained for regional and global applications.

4.2. Flow Velocity Estimation

[17] The flow velocity v_0 is unknown for most rivers and hydraulic regimes. A straightforward way to obtain v_0 estimates is by using the Manning formula [*Chow*, 1959; *Cunge et al*., 1980]. Assuming a rectangular river cross section, we have $v_0 = (1/\eta){y_0}^{2/3}{S_f}^{1/2}$, where η is the Manning roughness coefficient, and S_f is the friction slope of the given river reach. Although η is an empirical coefficient and its effective values are unknown for most rivers in the world, approximations can be skillfully guessed in some cases. *Chow* [1959] suggests that η can vary from 0.025 to 0.045 for large, straight, and full stage rivers, such as most mainstreams in the Amazon Basin. For this study, we adopted $\eta = 0.04$. The parameter S_f was approximated to the valley slope S_0, which was also derived from FLOW, based on SRTM elevations, as described in section 4.1. The friction slope may change seasonally, from high to low waters, while the valley slope is constant over time. This approximation leads us to the same assumption as in the kinematic wave equation that $S_f - S_0 = 0$. Since S_f changes are not available either in gridded forms or at a sufficient number of gauging stations, we assumed that the mean error considered in the sensitivity analysis (see section 4.3) can represent this seasonal change. Still assuming rectangular river cross sections, water depths can be defined as $y_0 = Q_{\text{mean}}/(v_0 W)$, and the Manning formula is rewritten as

$$v_0 = \left[\frac{1}{\eta}\left(\frac{Q_{\text{mean}}}{W}\right)^{2/3} S_f^{1/2}\right]^{3/5}. \quad (6)$$

[18] Estimated values of v_0 are presented in Figure 2e. Mean y_0 and v_0 values were calculated at each gauging station using the instantaneous in situ observations described in the previous section. Comparisons between estimated and mean observed y_0 and v_0 resulted in MAE values of 41% and 66%, respectively. The spatial distribution of MAE values for y_0 and v_0 is shown in Figures 4b and 4c. One can see that MAE distribution is quite random, and results cannot be related to any spatial propriety of the basin.

4.3. Uncertainty Analysis

[19] Since the data used in this paper are mostly derived from global data sets and empirical regressions, the uncertainty of the input variables and its impacts on the flow dynamics' classification must be taken into account. To address this issue, a sensitivity analysis was performed based on the following steps: for a given variable x with reference value x^*, a range RA (%) representing its uncertainty is chosen and sorted uniformly using $n = 11$ values from $(1 - \text{RA})x^*$ to $(1 + \text{RA})x^*$. Then, the river flow classification is conducted using not only the reference value but also $n \times m$ combinations of possible input variables, where m is the number of input variables. In this sense, it is possible to identify the most likely flood wave type and its probability to occur in each grid cell. According to equations (3) and (4), four input variables are used to determine the flood wave types ($m = 4$). Their respective uncertainty ranges RA are defined as the aforementioned MAE values, i.e., 44% (t_p), 66% (v_0), and 41% (y_0). As for S_{f0}, we adopted the uncertainty of 10%, similar to *LeFavour and Alsdorf* [2005] for river slopes derived from the FLOW algorithm in the Amazon main stream to account for the SRTM DEM errors.

5. Results

5.1. Flood Wave Type Map

[20] According to Figure 5a, most rivers of the Amazon Basin (~99%) can be represented by kinematic (KI) or diffusive (DF) wave equations. Rivers located in the headwaters and regions with larger slopes, such as in the Andean region, exhibit a KI flow type. These rivers represent 64.5% of the Amazon Basin. Main tributaries and also rivers with low slope, located mainly in the central part of the basin in Brazil, but also in Bolivian (llanos de Moxos) and Peruvian wetlands, are characterized by the presence

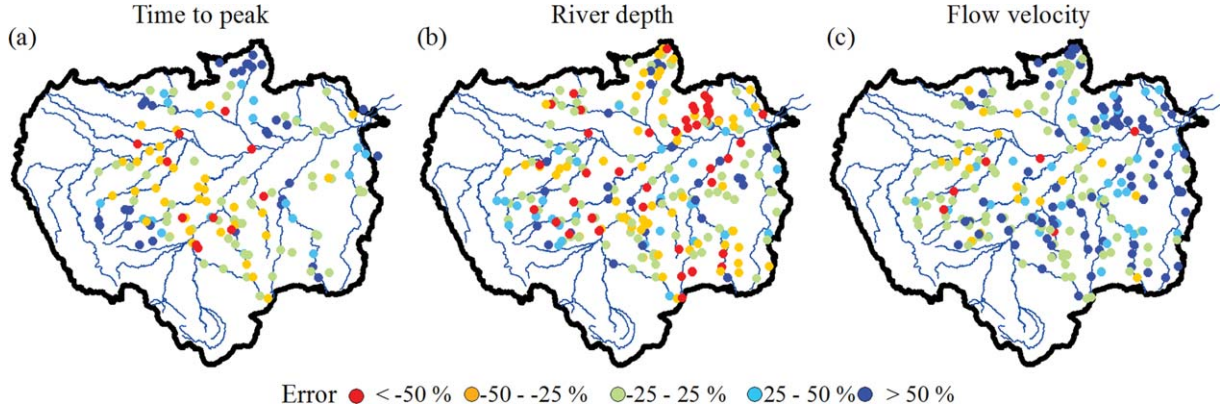

Figure 4. Spatial distribution of MAE values for (a) time to peak, (b) river depth, and (c) flow velocity.

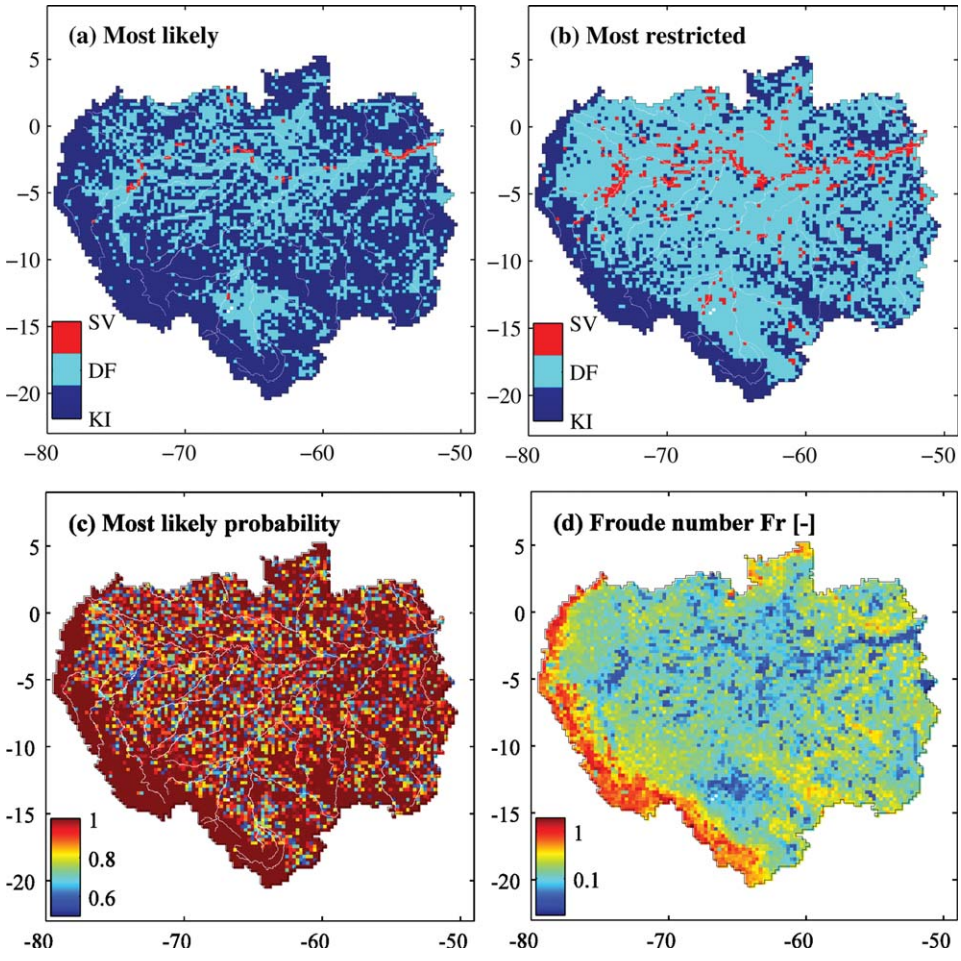

Figure 5. (a) Most likely and (b) most restricted flood wave type, (c) frequency of the most probable class and (d) Froude number maps for the Amazon Basin. Flow dynamics are represented by the following flood wave types: kinematic wave (KI), diffusive wave (DF), steady dynamic wave (SD), gravity wave (GV), and full Saint-Venant (SV). The white lines represent the main rivers.

of a DF flow (∼34.5% of the basin). Our results show the presence of a diffusive wave flow type in the major tributaries and agree with observational studies such as *Kosuth et al*. [2009] and *Meade et al*. [1991], showing the presence of backwater effects in the Solimões, central Amazon, Negro, Madeira, and Purus Rivers. It is also in accordance with a classification performed by *Trigg et al*. [2009] at a river reach in the Solimões/Amazon main stream. Full Saint-Venant hydrodynamic flow is present in the lower Amazon River where tidal effects were demonstrated by *Kosuth et al*. [2009] and also in some limited areas of the upper Solimões and Japurá Rivers (∼1% of the basin). The presence of SV flow is mainly due to low local slopes in these areas. For example, the grid cell representing the Obidos station has $S_f = 3 \times 10^{-6}$ m m^{-1}, resulting in low F_0^2 and T_+ values (0.004 and 0.8, respectively). It is important to note that changes in S_f values during a flood event can be higher than the value used to represent the uncertainty of friction slopes, i.e., 10%. This indicates that the SV flow can occur but the classification is still uncertain. Both gravity wave and steady dynamic wave flows do not show in any part of the basin.

[21] The uncertainties of variables used in equations (3) and (4) have low impact on the flood wave classification of most grid cells. According to the uncertainty analysis (Figure 5c), about 43% of grid cells have constant flood wave types, where 33% of them are KI and 10% DF. Also, the frequency of the most likely classification is larger than 80% in 76% of the cases, where 51% are controlled by the kinematic wave, ∼35% by the diffusive wave, and ∼0.1% by the full Saint-Venant equations.

[22] In order to obtain a more rigorous interpretation of the results, the upper limit of the sensitivity analysis was also evaluated. In this sense, a map containing the most complete forms of the Saint-Venant equations attributed to each grid cell was created and examined. As one can see in Figure 5b, an important part of the Amazon Basin is characterized by a diffusive wave flow type (∼62%). A significant increase of grid cells classified as SV is also noticed (∼5% of the Amazon Basin). SV flow is present at most of the Solimões/Amazon main stream but also at Jupurá River, in parts of the Negro and Branco Rivers and in the outlet of other main tributaries (Purus, Madeira, and Tapajós Rivers). In contrast, KI flow is predominant mostly at the Andean region (∼33%).

[23] Finally, we examined the flow dynamics of Amazonian rivers in terms of Froude number (Figure 5d). Most part of the basin is characterized by a subcritical flow

(99%), with very low *Fr* values (26.8% of grid cells present $Fr < 0.1$ and 92.7% $Fr < 0.5$). Lower *Fr* values are frequently found in the central Amazon Basin, along the Solimões/Amazon main stream, and in the southern and western parts of the basin, corresponding to the Bolivian and Peruvian wetlands, respectively. In contrast, large *Fr* values and supercritical flow ($Fr > 1$) are mostly observed in mountainous regions and clearly dominate the Andean part of the basin.

5.2. Evaluation Against In Situ Data

[24] In order to evaluate the flood wave type map, we identified the flow dynamics at selected gauging stations based mostly in available in situ data from discharge measurements campaigns. Equations (3) and (4) were used, replacing estimated y_0 and v_0 by observed values at 145 stream gauging stations, while t_p values were those obtained from daily discharge time series. S_f values were kept as those derived from satellite elevation because no observation of this variable is available. Taking advantage of a relatively large data set (~25,000 instant discharge measurements), the flow dynamics was classified for both the average of all observed variables at each station and the lowest and highest observed discharges, representing low and high water periods.

[25] According to Table 1, flood wave types remain the same during low and high water periods at most of the stations (~68%). For example, flood waves at Óbidos, located ~800 km upstream from the Amazon River mouth, are classified as SV for any discharge measurement. Water slope is low ($\sim 3 \times 10^{-6}$ m m^{-1}), and the flow regime is characterized as subcritical, with low F_0 values (0.06–0.10). Flow dynamics at Manacapuru station, located in the Solimões River ($S \approx 2 \times 10^{-5}$ m m^{-1}), upstream the confluence with the Negro River, is classified as DF in all cases and also has low F_0 values (0.07–0.12). Results from both sites are similar to those presented in the flood wave type map. On the other hand, high waters are better described by more complex forms of the Saint-Venant equations at approximately half of the remaining stations (~16%).

[26] Table 2 presents the distribution of flood wave type for the gauging stations based on discharge measurements and the respective grid cell from the flood wave type map (Figure 5a). KI, DF, and SV flood wave classes represent ~31%, ~65%, and ~4% of the gauging stations, respectively. Selected grid cells had similar results, with ~44%, ~55%, and ~1%, respectively. Most significant differences were found at gauging stations classified as SV, where the flood wave map indicates a DF flow instead. Differing flood wave classes using in situ and gridded data sets are mostly attributed to errors in water depth and flow velocity estimates that can be higher than 50% at some gauging stations (see Figures 4b and 4c). A large number (83.4%) of coinciding gauging stations and grid cells have the same classification indicating the feasibility of the flood wave type map estimates. However, it must be highlighted that the gauging stations are not uniformly distributed within the Amazon Basin (they are concentrated in the Brazilian portion of the basin and absent in the Andean mountainous region and in some strongly backwater-affected rivers). In this sense, this comparison must be carefully considered. Another limitation concerns the use of satellite-based valley slope instead of friction slope data. In some cases, actual S_f values can significantly differ from those derived by the DEM as a function of both the season (e.g., flood peak or recession) and DEM errors. Although this comparison has some limitations, it is useful to verify that the uncertainty in flow parameters do not introduce major errors in the flood wave classification.

Table 1. Percentage of In Situ Gauging Stations Classified as Kinematic Wave (KI), Diffusive Wave (DF), or Full Saint-Venant (SV) During Low and High Water Periods

	High Water			
Low Water	KI	DF	SV	Total
KI	18.62	15.86	0.00	34.48
DF	10.34	47.59	0.00	57.93
SV	0.00	6.21	1.38	7.59
Total	28.96	69.66	1.38	

Table 2. Percentage of In Situ Gauging Stations and Corresponding Flood Wave Type Map Grid Cells Classified as Kinematic Wave (KI), Diffusive Wave (DF), or Full Saint-Venant (SV)

	Map			
In Situ	KI	DF	SV	Total
KI	31.03	0.00	0.00	31.03
DF	13.10	51.72	0.00	64.82
SV	0.00	3.45	0.69	4.14
Total	44.13	55.17	0.69	

6. Concluding Remarks

[27] In this paper, a flood wave classification method is adapted to large-scale applications. The approach was developed based on global data sets and stream gauge observations. Results presented in this study are the first insights toward a large- and global-scale mapping of flood wave classes which can potentially contribute to a deeper understanding of spatially distributed flow dynamics of large rivers. The Amazon Basin was selected for a first attempt because of the generally expected results in the main river reaches based on previous studies [*Meade et al*., 1991; *Trigg et al*., 2009; *Paiva et al*., 2013a, 2013b].

[28] Using a broad 0.25° spatial resolution data set of river flow characteristics (water discharge, flow velocity, and roughness coefficient) and geometry (river width, depth, and slope), we could not only confirm previous findings described in the literature but also identify new discernments concerning river flow hydraulics in the Amazon Basin. Results demonstrate that rivers located in mountainous areas, such as in the Andean region, exhibit a kinematic wave flow type (~64.5% of the basin). The main Amazonian tributaries, low-slope rivers, and wetland regions are characterized by the presence of a diffusive wave flow type (~34.5%), which agrees with previous observational studies [e.g., *Meade et al*., 1991]. Full Saint-Venant hydrodynamics are present mostly at the lower Amazon River but also in some restricted parts of other major tributaries (~1%).

[29] Most part of the Amazon Basin is characterized by a subcritical flow with very low Froude number values,

especially along the Solimões/Amazon main stream and the main wetlands. On the other hand, the Andean region is dominated by large *Fr* values, and supercritical flow is present. In a more rigorous interpretation of the sensitivity analysis (represented by the most restrictive case shown in Figure 5b), a significant part of the Amazon Basin is characterized by the diffusive wave, the Saint-Venant equations' hydrodynamics is present along most of the Solimões/Amazon main stream and some other reaches of the main tributaries, and the kinematic wave is limited to the Andean region. The classification corresponds to the main river reaches represented by the grid cell, and smaller rivers are not considered. In this sense, due to the coarse scale of the map, results should be interpreted carefully. For example, it is unlikely that supercritical flows occur along all river reaches at smaller scales within cells with $Fr > 1$ in Andean region. Different flood wave types or mixed super and subcritical flow can also occur in rivers at smaller scales not represented by the spatial resolution considered in this study.

[30] Comparisons between the resulting flood wave type map and a classification predominately based on in situ observations at stream gauging stations indicate the agreement between both estimates (83.4%) and the feasibility of the applied methodology. In most cases flood wave type remains the same during low and high water periods (~68% of the stations). However, it must be highlighted that the approach has a number of simplifications and uncertainties, and results should be interpreted and considered carefully. The flood wave classification method developed by *Moussa and Bocquillon* [1996] was first applied by the same authors in a single river reach where information about parameters was easily available. In this paper, we applied the same method, but using spatially distributed parameters derived from regionalization methods. Also, recent studies present new simplifications of the Saint-Venant equations considering the inertial term [*Bates et al*., 2010; *Almeida et al*., 2012]. This formulation is not included in the current classification approaches, comprising the one used in this paper, but should be considered in future formulations of flood wave classification. Regarding the river geometry, the proposed river width formulation assumes a simple power law increasing as a function of a constant β and mean water discharge. However, actual river widths also vary as a function of other geomorphological features such as local topography. Although recent efforts have been made toward the acquisition of more accurate estimates of *W* based on the satellite data processing [e.g., *Pavelsky and Smith*, 2008], no global river width data set is currently available. Considering the valley slope as an approximation of water slope can also result in high uncertainty. In this study, we defined the water slope uncertainty based only on the local random error in SRTM. Longer range spatially correlated errors [*Rodríguez et al*., 2006] were not considered, which can occasionally change the flow type and/or probability of occurrence in some reaches. In reaches classified as SV, for example, increasing S_{f0} values result in higher T_+, leading to simplified forms of the Saint-Venant equations (see Figure 1).

[31] The methodology described herein can be potentially applied to higher spatial resolutions, according to the modeling requirements. However, detailed information about smaller rivers would be needed. In this study, river width (*W*), depth (y_0), and time to peak (t_p) were represented by equations adapted to large-scale rivers. Even though global DEMs are available at high resolutions, the inaccuracy of DEM-based valley slopes can significantly increase as a function of the spatial resolution, preventing one to obtain such information at a more detailed spatial scale. Most large river basins in the world, including the Amazon, are poorly gauged, and deriving such spatially distributed high-resolution information can be a difficult task. Also, even if the data are available, different equations should be used to represent the highly heterogeneous physical processes occurring at smaller scales in large areas.

[32] Regardless of all aforementioned simplifications, results may guide the development of the next generation of large-scale river-flood models and should act as an indicator of the minimum physical complexity required to simulate the system. They indicate that these models must provide a diffusional flood wave type representation and ultimately be prepared for full hydrodynamic simulations with both subcritical and supercritical flows. Alternately, aiming at optimal computational costs, hybrid models that use particular flood wave simplifications adapted to different river reaches [e.g., *Paiva et al*., 2013a] could also be employed.

[33] **Acknowledgments.** R.P. is funded by CNPq (Conselho Nacional de Desenvolvimento Científico, Brazil). Grateful acknowledgments are due to D. Yamazaki for providing FLOW algorithm outputs and to W. Collischonn (IPH/UFRGS), M. Trigg (U. Bristol), P. Bates (U. Bristol), and three anonymous reviewers for their valuable comments. This study benefited from data made available by ANA.

References

Almeida, G. A. M., P. Bates, J. E. Freer, and M. Souvignet (2012), Improving the stability of a simple formulation of the shallow water equations for 2-D flood modeling, *Water Resour. Res.*, *48*, W05528, doi:10.1029/2011WR011570.

Arora, V. K., F. H. S. Chiew, and R. B. Grayson (1999), A river flow routing scheme for general circulation models, *J. Geophys. Res.*, *104*, 14,347–14,357.

Bates, P. D., M. S. Horritt, and T. J. Fewtrell (2010), A simple inertial formulation of the shallow water equations for efficient two-dimensional flood inundation modelling, *J. Hydrol.*, *387*, 33–45, doi:10.1016/j.jhydrol.2010.03.027.

Chow, V. T. (1959). *Open Channel Hydraulics*, McGraw-Hill Book, New York.

Chow, V. T. (1962), Hydrological determination of waterway areas for the design of drainage structures in small drainage basins, *Univ. of Ill. Eng. Exp. Stn. Bull. 462*, Urbana, Ill.

Coe, M. T., M. H. Costa, and E. A. Howard (2008), Simulating the surface waters of the Amazon River basin: Impacts of new river geomorphic and flow parameterizations, *Hydrol. Processes*, *22*(14), 2542–2553.

Cogley, J. G. (2003), GGHYDRO—Global hydrographic data, release 2.3, *Trent Tech. Note 2003-1*, 11 pp., Dep. of Geogr., Trent Univ., Peterborough, Canada.

Collischonn, W., D. G. Allasia, B. C. Silva, and C. E. M. Tucci (2007), The MGB-IPH model for large-scale rainfall-runoff modeling, *Hydrol. Sci. J.*, *52*, 878–895.

Cunge, J. A., F. M. Holly, and A. Verney (1980), *Practical Aspects of Computational River Hydraulics*, Pitman Adv. Publ. Program, London.

Decharme, B., R. Alkama, F. Papa, S. Faroux, H. Douville, and C. Prigent (2011), Global off-line evaluation of the ISBA-TRIP flood model, *Clim. Dyn.*, *38*, 1389–1412, doi:10.1007/s00382-011-1054-9.

Draper, N. R., and H. Smith (1998), *Applied Regression Analysis*, pp. 307–312, Wiley-Interscience, Hoboken, N. J.

Gedney, N., P. M. Cox, and C. Huntingford (2004), Climate feedback from wetland methane emission, *Geophys. Res. Lett.*, *31*, L20503, doi:10.1029/2004GL020919.

Getirana, A. C. V., A. Boone, D. Yamazaki, B. Decharme, F. Papa, and N. Mognard (2012), The Hydrological Modeling and Analysis Platform (HyMAP): Evaluation in the Amazon basin, *J. Hydrometeorol.*, *13*, 1641–1665.

Kiprich, Z. P. (1940), Time of concentration of small agricultural watersheds, *Civ. Eng.*, *10*(6), 362.

Kosuth, P., J. Callède, A. Laraque, N. Filizola, J. L. Guyot, P. Seyler, J. M. Fritsch, and V. Guimarães (2009), Sea-tide effects on flows in the lower reaches of the Amazon River, *Hydrol. Process.*, *23*(22), 3141–3150.

Krinner, G. (2003), Impact of lakes and wetlands on boreal climate, *J. Geophys. Res.*, *108*(D16), 4520, doi:10.1029/2002JD002597.

LeFavour, G., and D. Alsdorf (2005), Water slope and discharge in the Amazon River estimated using the Shuttle Radar Topography Mission digital elevation model, *Geophys. Res. Lett.*, *32*, L17404, doi:10.1029/2005GL023836.

Lehner, B., and P. Döll (2004), Development and validation of a global database of lakes, reservoirs and wetlands, *J. Hydrol.*, *296*, 1–22.

Liston, G. E., Y. C. Sud, and E. F. Wood (1994), Evaluating GCM land surface hydrology parameterizations by computing river discharges using a runoff routing model: Application to the Mississippi basin, *J. Appl. Meteorol.*, *33*, 394–405.

Loukas, A., and M. C. Quick (1996), Physically-based estimation of lag time for forested mountainous watersheds, *Hydrol. Sci. J.*, *41*(1), 1–19, doi:10.1080/02626669609491475.

Masutomi, Y., Y. Inui, K. Takahashi, and U. Matsuoka (2009), Development of highly accurate global polygonal drainage basin data, *Hydrol. Process.*, *23*, 572–584.

Meade, R. H., J. M. Rayol, S. C. Da Conceiȩão, and J. R. G. Natividade (1991), Backwater effects in the Amazon River basin of Brazil, *Environ. Geol. Water Sci.*, *18*(2), 105–114.

Moussa, R., and C. Bocquillon (1996), Criteria for the choice of flood routing methods in natural channels, *J. Hydrol.*, *186*, 1–30.

Natural Environment Research Council (1975), Flood Studies Report, Hydrological Studies, vol. 1, London, U. K.

Neal, J., I. Villanueva, N. Wright, T. Willis, T. Fewtrell, and P. Bates (2012), How much physical complexity is needed to model flood inundation?, *Hydrol. Process.*, *26*(15), 2264–2282, doi:10.1002/hyp.8339.

New, M., D. Lister, M. Hulme, and I. Makin (2002), A high-resolution data set of surface climate over global land areas, *Clim. Res.*, *21*(1), 1–25.

Oki, T., and S. Kanae (2006), Global hydrological cycles and world water resources, *Science*, *313*, 1068–1072, doi:10.1126/science.1128845.

Paiva, R. C. D., W. Collischonn, M. P. Bonnet, D. C. Buarque, F. Frappart, S. Calmant, and C. B. Mendes (2013a), Large scale hydrological and hydrodynamic modelling of the Amazon River basin, *Water Resour. Res.*, *49*, 2437–2445, doi:10.1002/wrcr.20067.

Paiva, R. C. D., W. Collischonn, and D. C. Buarque (2013b), Validation of a full hydrodynamic model for large scale hydrologic modelling in the Amazon, *Hydrol. Process.*, *27*(3), 333–346, doi:10.1002/hyp.8425.

Papa, F., C. Prigent, F. Aires, C. Jimenez, W. B. Rossow, and E. Matthews (2010), Interannual variability of surface water extent at the global scale, 1993–2004, *J. Geophys. Res.*, *115*, D12111, doi:10.1029/2009JD012674.

Pavelsky, T. M., and L. C. Smith (2008), RivWidth: A software tool for the calculation of river widths from remotely sensed imagery, *IEEE Geosci. Remote Sens. Lett.*, *5*(1), 70–73, doi:10.1109/LGRS.2007.908305.

Rodríguez, E., C. S. Morris, and J. E. Belz (2006), A global assessment of the SRTM performance, *Photogramm. Eng. Remote Sens.*, *72*(3), 249–260.

Tomasella, J., L. S. Borma, J. A. Marengo, D. A. Rodriguez, L. A. Cuartas, C. A. Nobre, and M. C. R. Prado (2010), The droughts of 1996–1997 and 2004–2005 in Amazonia: Hydrological response in the river main-stem, *Hydrol. Process.*, *25*(8), 1228–1242.

Trigg, M. A., M. D. Wilson, P. D. Bates, M. S. Horritt, D. E. Alsdorf, B. R. Forsberg, and M. C. Vega (2009), Amazon flood wave hydraulics, *J. Hydrol.*, *374*, 92–105, doi:10.1016/j.jhydrol.2009.06.004.

Vieira, J. H. D. (1983), Conditions governing the use of approximations for the Saint-Venant equations for shallow surface-water flow, *J. Hydrol.*, *60*(1–4), 43–58.

Vorosmarty, C. J., B. Moore, A. L. Grace, M. P. Gildea, J. M. Melillo, B. J. Peterson, E. B. Rastetter, and P. A. Steudler (1989), Continental scale models of water balance and fluvial transport: An application to South America, *Global Biogeochem. Cycles*, *3*, 241–265.

Watt, W. E., and K. C. A. Chow (1985), A general expression for basin lag time, *Can. J. Civ. Eng.*, *12*, 294–300.

Yamazaki, D., T. Oki, and S. Kanae (2009), Deriving a global river network map and its sub-grid topographic characteristics from a fine-resolution flow direction map, *Hydrol. Earth Syst. Sci.*, *13*, 2241–2251, doi:10.5194/hess-13–2241-2009.

Yamazaki, D., S. Kanae, K. Hyungjun, and T. Oki (2011), A physically-based description of floodplain inundation dynamics in a global river routing model, *Water. Resour. Res.*, *47*, W04501, doi:10.1029/2010WR009726.

Yamazaki, D., C. Baugh, P. D. Bates, S. Kanae, D. E. Alsdorf, and T. Oki (2012), Adjustment of a spaceborne DEM for use in floodplain hydrodynamic modelling, *J. Hydrol.*, *436–437*, 81–91, doi:10.1016/j.jhydrol.2012.02.045.